Ground-based remote sensing of wind by heterodyne pulsed Doppler lidar

(Draft text of the common ISO/WMO standard 28902-2:2016(E))

Introduction

Lidars ("LIght Detection And Ranging"), standing for atmospheric lidars in the scope of this document have proven to be valuable systems for remote sensing of atmospheric pollutants, of various meteorological parameters such as clouds, aerosols, gases and (where Doppler technology is available) wind. The measurements can be carried out without direct contact and in any direction as electromagnetic radiation is used for sensing the targets. Lidar systems, therefore, supplement the conventional in-situ measurement technology. They are suited for a large number of applications that cannot be adequately performed by using in situ or point measurement methods.

There are several methods by which lidar can be used to measure atmospheric wind. The four most commonly used methods are pulsed and continuous wave coherent Doppler wind lidar, direct-detection Doppler wind lidar and resonance Doppler wind lidar (commonly used for mesospheric sodium layer measurements). For further reading, please refer e.g. to [1] and [2].

This annex[1] describes the use of heterodyne pulsed Doppler lidar systems. Some general information on continuous-wave Doppler lidar can be found in Attachment A. An International Standard on this method is in preparation.

1 Scope

This annex specifies the requirements and performance test procedures for heterodyne pulsed Doppler lidar techniques and presents their advantages and limitations. The term "Doppler lidar" used in this annex applies solely to heterodyne pulsed lidar systems retrieving wind measurements from the scattering of laser light onto aerosols in the atmosphere. A description of performances and limits are described based on standard atmospheric conditions.

This annex describes the determination of the line-of-sight wind velocity[2] (radial wind velocity).

This annex does not address the retrieval of the wind vector.

This annex may be used for the following application areas:

— meteorological briefing for e.g. aviation, airport safety, marine applications, oil platforms;

— wind power production, e.g. site assessment, power curve determination;

— routine measurements of wind profiles at meteorological stations;

— air pollution dispersion monitoring;

— industrial risk management (direct data monitoring or by assimilation into micro-scale flow models);

— exchange processes (greenhouse gas emissions).

This annex addresses manufacturers of heterodyne pulsed Doppler wind lidars as well as bodies testing and certifying their conformity. Also, this document provides recommendations for the users to make adequate use of these instruments.

[1] Whereas this is referred to as an annex in the WMO *Guide to Meteorological Instruments and Methods of Observation* (WMO-No. 8), it is referred to as a standard in the ISO document.

[2] Derivation of wind vector from individual line of sight measurements is not described in this annex since it is highly specific to a particular wind lidar configuration. One example of the retrieval of the wind vector can be found in Attachment B.

2 Terms and definitions

For the purposes of this document, the following terms and definitions apply.

2.1
data availability
ratio between the actual considered measurement data with a predefined data quality and the number of expected measurement data for a given measurement period

2.2
displayed range resolution
constant spatial interval between the centres of two successive range gates

Note 1 to entry: The displayed range resolution is also the size of a range gate on the display. It is determined by the range gate length and the overlap between successive gates.

2.3
effective range resolution
application-related variable describing an integrated range interval for which the target variable is delivered with a defined uncertainty

2.4
effective temporal resolution
application-related variable describing an integrated time interval for which the target variable is delivered with a defined uncertainty

2.5
extinction coefficient, α
measure of the atmospheric opacity, expressed by the natural logarithm of the ratio of incident light intensity to transmitted light intensity, per unit light path length

2.6
integration time
time spent in order to derive the line of sight velocity

2.7
maximum acquisition range, R_{MaxA}
maximum distance to which the lidar signal is recorded and processed

Note 1 to entry: It depends on the number of acquisition points and the sampling frequency

2.8
minimum acquisition range, R_{MinA}
minimum distance from which the lidar signal is recorded and processed

Note 1 to entry: If the minimum acquisition range is not given, it is assumed to be zero. It can be different from zero, when the reception is blind during the pulse emission.

2.9
maximum operational range, R_{MaxO}
maximum distance to which a confident wind speed can be derived from the lidar signal

Note 1 to entry: The maximum operational range is less than or equal to the maximum acquisition range.

Note 2 to entry: The maximum operational range is defined along an axis corresponding to the application. It is measured vertically for vertical wind profiler. It is measured horizontally for scanning lidars able to measure in the full hemisphere.

Note 3 to entry: The maximum operational range can be increased by increasing the measurement period and/or by downgrading the range resolution.

Note 4 to entry: The maximum operational range depends on lidar parameters but also on atmospheric conditions.

2.10
measurement period
interval of time between the first and last measurements

2.11
minimum operational range, R_{MinA}
minimum distance where a confident wind speed can be derived from the lidar signal

Note 1 to entry: The minimum operational range is also called blind range.

Note 2 to entry: In pulsed lidars, the minimum operational range is limited by the stray light in the lidar during pulse emission, by the depth of focus, or by the detector transmitter/Receiver switch time. It can depend on pulse duration (tp) and range gate width (RGW).

2.12
physical range resolution
width (FWHM) of the range weighting function

2.13
range gate
width (FWHM) of the weighting function selecting the points in the time series for spectral processing and wind speed computation

Note 1 to entry: The range gate is centred on the measurement distance.

Note 2 to entry: The range gate is defined in number of bins or equivalent distance range gate.

2.14
range resolution
equipment-related variable describing the shortest range interval from which independent signal information can be obtained

2.15
range weighting function
weighting function of the radial wind speed along the line of sight

2.16
temporal resolution
equipment-related variable describing the shortest time interval from which independent signal information can be obtained

2.17
velocity bias
maximum instrumental offset on the velocity measurement

Note 1 to entry: The velocity bias has to be minimized with adequate calibration, for example on a fixed target.

2.18
velocity range
range determined by the minimum measurable wind speed, the maximum measurable wind speed and the ability to measure the velocity sign, without ambiguity

Note 1 to entry: Depending on the lidar application, velocity range can be defined on the radial wind velocity (scanning lidars) or on horizontal wind velocities (wind profilers).

2.19
velocity resolution
instrumental velocity standard deviation

Note 1 to entry: The velocity resolution depends on the pulse duration, the carrier to noise ratio and integration time.

2.20
wind shear
variation of wind speed across a plane perpendicular to the wind direction

3 Fundamentals of heterodyne pulsed Doppler lidar

3.1 Overview

A pulsed Doppler lidar emits a laser pulse in a narrow laser beam (see Figure 1). As it propagates in the atmosphere, the laser radiation is scattered in all directions by aerosols and molecules. Part of the scattered radiation propagates back to the lidar, it is captured by a telescope, detected and analysed. Since the aerosols and molecules move with the atmosphere, a Doppler shift results in the frequency of the scattered laser light.

At the wavelengths (and thus frequencies) relevant to heterodyne (coherent) Doppler lidar it is the aerosol signal that provides the principle target for measurement of the back-scattered signal.

The analysis aims at measuring the difference Δf between the frequencies f_t of the emitted laser pulse and f_r of the backscattered light. According to the Doppler's equation, this difference is proportional to the line-of- sight wind component:

$$\Delta f = f_r - f_t = -2v_r/\lambda \quad (1)$$

Where

λ is the laser wavelength;

v_r is the line-of-sight wind component (component of the wind vector $\vec{v}$ along the axis of laser beam, counted positive when the wind is blowing away from the lidar).

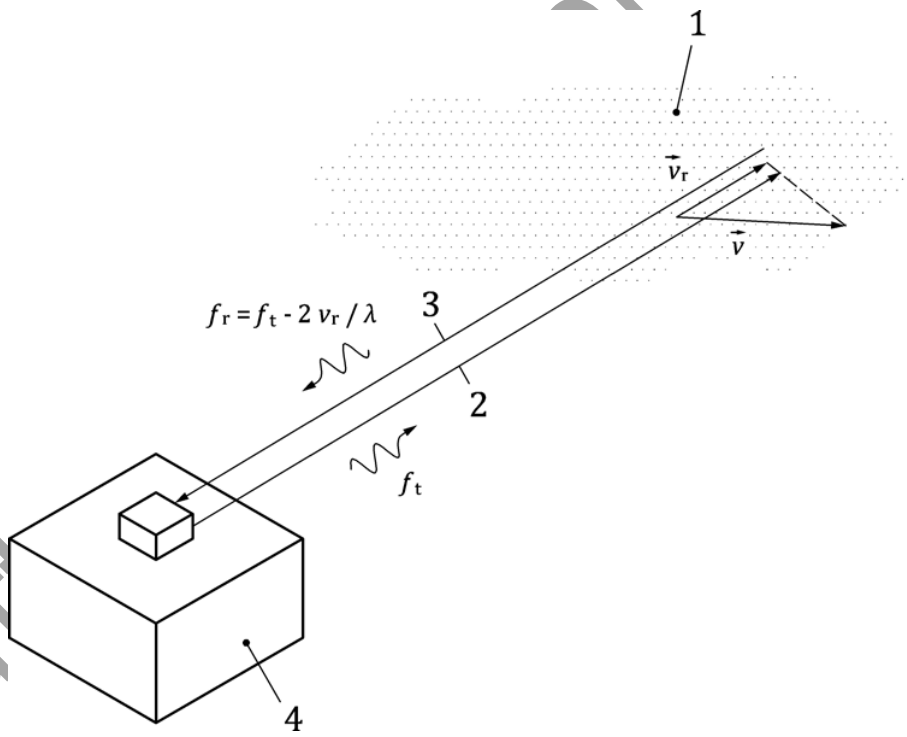

Key

1 Scattering particles moving with the wind

2 Optical path of the emitted laser pulse (laser beam)

3 Optical axis of the receiver

4 Lidar instrument

Figure 1— Measurement principle of a heterodyne Doppler lidar: A laser pulse is emitted and propagates in the atmosphere. Aerosol particles and molecules scatter the laser light in all directions. At the wavelengths normally exploited by coherent Doppler wind lidar systems, the aerosol particles provide the back-scattered signal that can be exploited for Doppler wind measurements. The light scattered backwards is collected by a telescope, detected and analysed. The analysis aims at measuring the frequency Doppler shift between emission and reception. The Doppler shift is proportional to the line-of-sight wind component.

The measurement is range resolved as the backscattered radiation received at time t after the emission of the laser pulse has travelled from the lidar to the aerosols at range x and back to the lidar at the speed of light c. Formula (2) shows the linear relationship between range and time.

$$x = c \cdot \frac{t}{2} \tag{2}$$

3.2 Heterodyne detection

In a heterodyne lidar, the detection of the light captured by the receiving telescope (at frequency $f_r = f_t + \Delta f$) is described schematically in Figure 2. The received light is mixed with the beam of a highly stable, continuous-wave laser called the local oscillator. The sum of the two electromagnetic waves – backscattered and local oscillator – is converted into an electrical signal by a quadratic detector (producing an electrical current proportional to the power of the electromagnetic wave illuminating its sensitive surface). An analogue, high-pass filter is then applied for eliminating the low-frequency components of the signal.

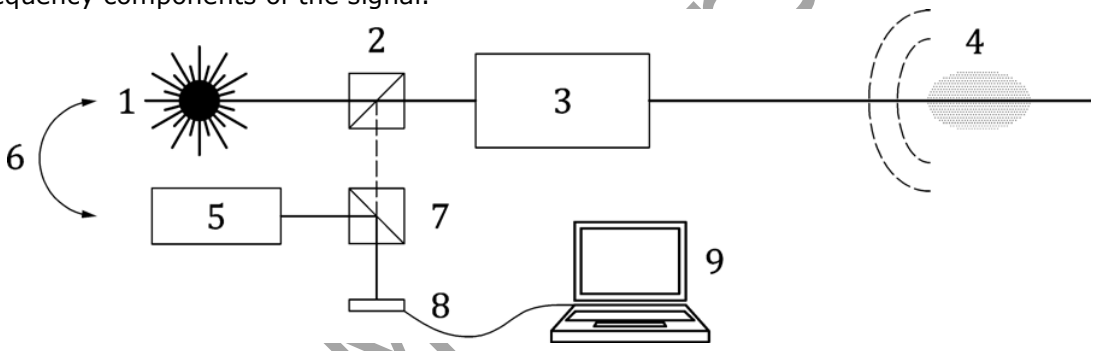

Key

———	Optical path of the emitted laser pulse (radiation at frequency f_t)
- - - -	Optical path of the received light (radiation at frequency $f_t + \Delta f$)
———	Beam of the local oscillator laser (radiation at frequency f_{lo})
1	Pulsed laser
2	Optical element separating the received and emitted lights
3	Telescope (used for transmitting and receiving)
4	Scatterers
5	Local oscillator laser (continuous wave laser)
6	Frequency control loop. This device sets the difference f_t-f_{lo}
7	Optical element aligning the beam of the local oscillator along the optical axis of the received light beam and mixing them together
8	Quadratic detector
9	Analog to digital converter and digital signal processing unit

Figure 2 — Principle of the heterodyne detection

The result is a current $i(t)$ beating at the radio frequency $f_t + \Delta f - f_{lo}$):

$$\underbrace{i(t) = 2 \cdot \frac{\eta \cdot e}{h \cdot f_t} \cdot K \cdot \xi(t) \cdot \sqrt{\gamma(t) \cdot P_r(t) \cdot P_{lo}} \cdot \cos\left(2\pi(\Delta f + f_t - f_{lo}) \cdot t + \varphi(t)\right) + n(t)}_{i_{het}(t)} \quad (3)$$

Where

t is the time;

h is the Planck constant;

η is the detector quantum efficiency;

e is electrical charge of an electron;

K is the instrumental constant taking into account transmission losses through the receiver;

$\xi(t)$ is the random modulation of the signal amplitude by speckles effect (see Clause 5.3.2);

$\gamma(t)$ is the heterodyne efficiency;

$P_r(t)$ is the power of the backscattered light;

P_{lo} is the power of the local oscilator;

f_{lo} is the frequency of the local oscilator;

$\varphi(t)$ is the random phase;

$n(t)$ is the white detection noise;

$i_{het}(t)$ is the heterodyne signal.

The heterodyne efficiency $\gamma(t)$ is a measure for the quality of the optical mixing of the backscattered and the local oscillator wave fields on the surface of the detector. It cannot exceed 1. A good heterodyne efficiency requires a careful sizing and alignment of the local oscillator relative to the backscattered wave. Optimal mixing conditions are discussed in [3]. The heterodyne efficiency is not a purely instrumental function, it also depends on the refractive index turbulence (Cn^2) along the laser beam (see [4]). Under conditions of strong atmospheric turbulence, the effect on varying the refractive index degrades the heterodyne efficiency. This can happen when the lidar is operated close to the ground during a hot sunny day.

In Formula (4) $P_r(t)$ is the instantaneous power of the backscattered light. It is given by the lidar equation (see [3])

$$P_r(t) = A \cdot \int_0^{+\infty} x^{-2} \cdot G(x) \cdot g\left(t - \frac{2x}{c}\right) \cdot \beta(x) \cdot \tau^2(x)\, dx \quad (4)$$

With

$$\tau(x) = exp\left(-\int_0^x \alpha(\zeta) d\zeta\right)$$

Where

x is the distance to the lidar

A is the collecting surface of the receiving telescope

$G(x)$ is the range-dependent sensitivity function ($0 \leq G(x) \leq 1$) taking into account e.g. the attenuation of the receiver efficiency at short range to avoid the saturation of the detector.

$g(t)$ is the envelope of the laser pulse power ($\int g(t)dt = E_0$ with E_0 the energy of the laser pulse)

$\beta(x)$ is the backscatter coefficient of the probed atmospheric target

$\tau(x)$ is the atmospheric transmission as a function of the extinction coefficient α

3.3 Spectral analysis

The retrieval of the radial velocity measurement from heterodyne signals requires a frequency analysis. This is done in the digital domain after analog-to-digital conversion of the heterodyne signals. An overview of the processing is given in Figure 3. The frequency analysis is applied to a time window $[t, t + \Delta t]$ and is repeated for a number *N* of lidar pulses. The window defines a range gate $[x, x + \Delta x]$ with $x = c \cdot t / 2$ and $\Delta x = c \cdot \Delta t / 2$. *N* is linked to the integration time $t_{int} = 1/f_{PRF}$ of the measurement (f_{PRF} is the pulse repetition frequency). The signal analysis consists in averaging the power density functions of the range gated signals. A frequency estimator is then used for estimating the central frequency of the signal peak. It is an estimate $\hat{f}_{het}$ for the frequency $f_{het} = \Delta f + f_t - f_{lo}$ of the heterodyne signal (see Figure 3).

Due to the analog to digital conversion, the frequency interval resolved by the frequency analysis is limited to [0, +*F*s/2] or [-*F*s/2, +*F*s/2] for complex valued signals. This limits the minimum and maximum values of $\hat{f}_{het}$ and thus the interval of measurable radial velocities. As shown in [5] Formula (5) estimates a range-gate average of the true wind radial velocity:

$$\hat{v}_r = -\frac{\lambda}{2}\left(\hat{f}_{het} - f_t + f_{lo}\right) \tag{5}$$

For instance, in the case the signal is real valued (no complex-demodulation), the frequency offset $f_t - f_{lo}$ is set to about $F_s/4$, so $|\hat{v}_r| \leq \lambda F_s/8$. Alternatively, a system specification requiring the possibility to measure radial winds up to v_{max} commands $F_s \geq 8v_{max}/\lambda$.

The averaging kernel is the convolution function between the pulse profile and the range-gate profile. Its length is a function of the pulse footprint in the atmosphere Δr (see Formula (6)), of the range gate Δx and of the weighting factor κ, where κ is the ratio between the gate full width at half maximum (FWHM) and Δx.

$$\Delta r = \frac{c \cdot T_p}{2} \tag{6}$$

Where

T_p is the FWHM duration of the laser pulse instantaneous intensity

The range resolution ΔR is defined as the FWHM of the averaging kernel. For a Gaussian pulse and an unweighted range gate, ΔR is equal to [6]:

$$\Delta R = \frac{c}{2} \cdot \frac{\Delta t}{erf\left(\frac{\sqrt{\pi} \cdot \Delta t}{2T_p}\right)} = \frac{\Delta x}{erf\left(\frac{\sqrt{\pi} \cdot \Delta x}{2\Delta r}\right)} \tag{7}$$

For a Gaussian pulse and a Gaussian weighted range gate, ΔR is equal to:

$$\Delta R = \frac{c}{2} \cdot \sqrt{T_p^2 + (\kappa \cdot \Delta t)^2} = \sqrt{\Delta r^2 + (\kappa \cdot \Delta x)^2} \tag{8}$$

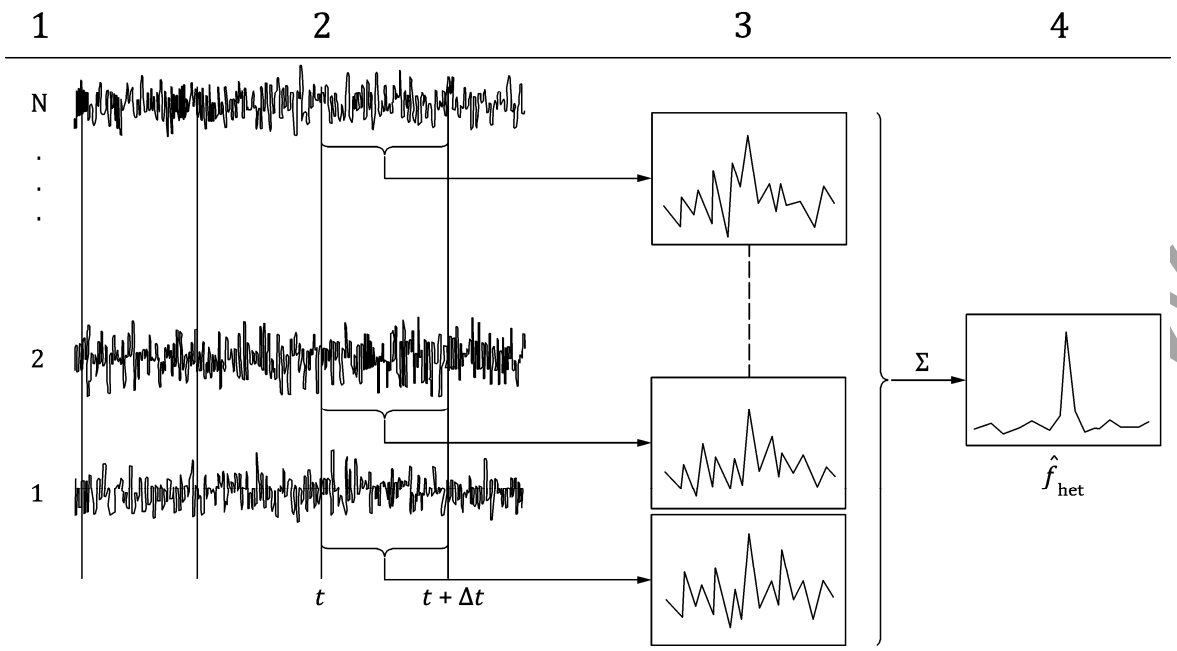

Key

t	time elapsed since the emission of the laser pulse
Δt	duration of the spectral analysis time window. It sets the size of the range gate
N	signal number
1	pulses
2	time series
3	spectra
4	Doppler frequency

Figure 3—Diagram showing how the frequency analysis is conducted. Several signals are considered and range gated. The average spectrum (grey line) is computed and a frequency estimator is applied.The black line shows the shape of the mean spectrum

Successive range gates can be partially overlapping (then successive radial velocity measurements are partially correlated) adjacent or disjoint (then there is a "hole" in the line-of-sight profile of the radial velocity).

Several possible frequency estimators are presented in [6] with a first analysis of their performances. Their performances are further discussed in [7]. Whatever the estimator, the probability density function of the estimates is the sum of a uniform distribution of "bad" estimates (gross errors) spread across the entire band $[-f_{max}, f_{max}]$ and a relatively narrow distribution of good estimates often modelled by a Gaussian distribution

$$p(\hat{f}_{het}) = \begin{cases} \frac{b}{2f_{max}} + \frac{1-b}{\sqrt{2\pi}\sigma_f} exp\left(-\frac{(\hat{f}_{het}-\bar{f}_{het})^2}{2\sigma_f^2}\right), for\ \hat{f}_r \in [-f_{max}, f_{max}] \\ 0\ otherwise \end{cases} \quad (9)$$

In principle, the mean frequency $\bar{f}_{het}$ can be different from the "true" heterodyne signal frequency f_{het}. This can happen for instance when the frequency drifts during the laser pulse (chirp, see [8]). However, these conditions are rarely met and a good heterodyne Doppler lidar produces in practice un-biased measurements of Doppler shifts.

The parameter σ_f characterizes the frequency precision of the estimator. The corresponding radial velocity precision is $\sigma_v = \lambda \cdot \sigma_f/2$. In a heterodyne system, it is typically of the order of several to

several tens of centimetres per second. It degrades with the level of noise (power of $n(t)$ in Formula (3)) and improves with the number of accumulated signals N. In practice the improvement is limited as the accumulation of a large number of signals result in a long integration time during which the natural variability (turbulence) of the wind increases.

[9] discusses the presence of gross errors (also called outliers [1]) and proposes a model for the parameter b as a function of the several instrument characteristics and the level of detection noise. An outlier happens when the signal processor detects a noise peak instead of a signal peak. The parameter b is a decreasing function of the CNR. Quality checks shall be implemented in heterodyne lidar systems so gross errors are filtered out and ignored as missing data. The presence of gross errors sets the maximum range of the lidar.

3.4 Target variables

The aim of heterodyne Doppler wind lidar measurements is to characterize the wind field. In each range interval, the evaluation of the measured variable leads to the radial velocity (Formula (5)).

There are additional target values like the variability of the radial velocity that are not discussed in this annex.

The target variables can be used as input to different retrieval methods to derive meteorological products like the wind vector at a point or on a line (profile), in an arbitrary plane or in space as a whole. This also includes the measurement of wind shears, aircraft wake vortices, updraft and downdraft regions of the wind. An additional aim of the Doppler wind lidar measurements is to determine kinematic properties and parameters of inhomogeneous wind fields such as divergence and rotation. See examples of applications in Attachment C.

3.5 Sources of noise and uncertainties

3.5.1 Local oscillator shot noise

The shot noise is denoted $n(t)$ in Formula (3). Its variance is proportional to the Local Oscillator (LO) power.

$$\langle n_{SN}^2 \rangle = 2eSP_{lo}B \qquad (10)$$

Where

S is the detector sensitivity, $S = \frac{\eta e}{hf_t}$, where η is the detector quantum efficiency;

B is the detection bandwidth.

It causes gross errors and limits the maximum range of the signal. If no other noise source prevails, the strength of the heterodyne signal relative to the level of noise is measured by the Carrier to noise Ratio *CNR* (see Equation (4) in [6])

$$CNR = \frac{\eta \cdot K \cdot \gamma(t)}{h \cdot f_t \cdot B} P_r(t) \qquad (11)$$

NOTE: Some authors sometimes call SNR (Signal to noise ratio) what is defined here as the Carrier to noise ratio (CNR).

3.5.2 Detector noise

Additional technical sources of noise can affect the SNR. As the shot noise, their spectral density is constant along the detection bandwidth (white noise).

— Dark noise is created by the fluctuations of the detector dark current i_D:

$$\langle n_{DN}^2 \rangle = 2ei_D B \quad (12)$$

— Thermal noise (Johnson/Nyquist noise) is the electronic noise generated by the thermal agitation of the electrons inside the load resistor R_L at temperature T:

$$\langle n_{TN}^2 \rangle = \frac{4k_B T}{R_L} B \quad (13)$$

Where

k_B is the Boltzman constant

3.5.3 Relative intensity noise (RIN)

The RIN (dB/Hz) is the LO power noise normalized to the average power level. RIN typically peaks at the relaxation oscillation frequency of the laser then falls off at higher frequencies until it converges to the shot noise level. (Pink noise). The RIN noise current increases with the square of LO power.

$$n_{RIN}^2 = (SP_{lo})^2 10^{0.1RIN} B \quad (14)$$

In a good lidar system, i_D, RIN, 1/RL are low enough so that the LO shot noise is the prevailing source of noise. In that case only, Equation 14 is applicable.

3.5.4 Speckles

The heterodyne signal for a coherent Doppler wind lidar is the sum of many waves backscattered by individual aerosol particles. As the particles are randomly distributed along the beam in volumes much longer than the laser wavelength, the backscattered waves have a random phase when they reach the sensitive surface of the detector. They thus add randomly. As a result, the heterodyne signal has a random phase and amplitude. The phenomenon is called speckles (see [10]). It limits the precision of the frequency estimates.

3.5.5 Laser frequency

A precise measurement of the radial velocity requires an accurate knowledge of $f_r - f_{lo}$. Any uncertainty in this value results in a bias in $\hat{f}_r$. If the laser frequency f_t is not stable, it should either be measured or locked to f_{lo}.

3.6 Range assignment

The range assignment of Doppler measurements is based on the time elapsed since the emission of the laser pulse. This time must be measured with a good accuracy (the error εt must be smaller or equal than $2\delta \cdot x/c$ where $\delta \cdot x$ is the required precision on the range assignment). This requires in particular that the time of the laser pulse emission is determined with at least this precision.

3.7 Known limitations

Doppler lidars rely on aerosol backscatter. Aerosols are mostly generated at ground and lifted up to higher altitudes by convection or turbulence. They are therefore in great quantities in the planetary boundary layer (typically 1000 meters thick during the day in tempered areas, 3000 meters in tropical regions), but in much lower concentrations above. It follows Doppler lidars hardly measure winds above the planetary boundary layer except in the presence of higher altitude aerosol layers like desert dusts or volcanic plumes.

Laser beams are strongly attenuated in fogs or in clouds. It follows the maximum range of Doppler lidars is strongly limited in fogs (a few hundreds of meters at best) and cannot measure winds inside or beyond a cloud. They are able to penetrate into subvisible clouds as cirrus clouds. Therefore wind information at high altitude (8 km to 12 km) can be retrieved from crystal particle

backscattering.

Doppler lidars detect cloud water droplets or ice crystals when they are present in the atmosphere. As they are efficient scatterers, they may dominate the return from the atmosphere, in case of heavy precipitation for example, in which case the Doppler lidar measures the radial velocity of hydrometeors rather than the radial wind.

Rain downwashes the atmosphere, bringing aerosols to the ground. The range of a Doppler lidar is generally significantly reduced after a rain, before the aerosols are lifted again.

The presence of rain water on the window of a Doppler lidar strongly attenuates its transmission. Unless a lidar is equipped with a wiper or a blower, its window must be wiped manually.

As explained in Clause 3.2, the efficiency of heterodyne detection is degraded by the presence of refractive index turbulence along the beam. Refractive index turbulence is mostly present near the surface during sunny days. The maximum range of Doppler lidar looking horizontally close to the surface may thus be substantially degraded in such conditions.

4 System specifications and tests

4.1 System specifications

4.1.1 Transmitter characteristics

4.1.1.1 Laser wavelength

The laser wavelength depends mainly on the technology used to build the laser source. Most of the existing techniques use near-infrared wavelengths between 1.5 µm to 2.1 µm, even though other wavelengths up to 10.6 µm may be used. The choice of the wavelength takes into account the expected power parameters but also the atmospheric transmission and the laser safety (see [11] and [12]). In fact the choice of the window between 1.5 µm and 2.1 µm is a compromise between technology and safety considerations (> 1.4 µm to ensure eye safety).

4.1.1.2 Pulse duration

The laser pulse duration T_p is the FWHM of the laser pulse envelope $g(t)$. T_p defines the atmosphere probed length R_p contributing to the instantaneous lidar signal:

$$R_p = \frac{c \cdot T_p}{2} \quad (15)$$

As an example, a pulse duration of 200 ns corresponds to a probed length of approx. 30 m.

4.1.1.3 Velocity precision and range resolution vs. pulse duration

There is a critical relationship between the pulse duration and two performance-related features. A long pulse duration of several hundreds of nanoseconds leads to a potentially narrow FWHM of the laser pulse spectrum (if "chirping" can be avoided), (see the Fourier-transform of the overall pulse in the time-domain). This can lead to a very accurate wind measurement even for a very low signal to noise ratio provided that outliers can be avoided (see Clause 3.3). There is an adverse impact from high performance on range resolution. A pulse duration of 1 µs limits the effective range resolution to approx. 150 m (see Formula (6)).

4.1.1.4 Pulse repetition frequency

The pulse repetition frequency f_{PRF} is the laser pulse emission frequency. f_{PRF} determines the number of pulses sent and averaged per line of sight in the measurement time. It also determines the maximum unambiguous range where the information of two consecutive sent laser pulses will not overlap. The maximum unambiguous range R_{MaxO} corresponding to f_{PRF} as in Formula (16)

$$R_{MaxO} = \frac{c}{2 f_{PRF_{max}}} \quad (16)$$

For example, for a maximum operational range of 15 km, the maximum f_{PRF} is 10 kHz.
As for radars however, specific types of modulation (carrier frequency, repetition frequency, …) can overcome the range ambiguity beyond R_{MaxO}.

4.1.2 Transmitter/receiver characteristics

The transmitter/receiver is defined at least by the parameters given in Table 1.

Table 1 — Transmitter/receiver characteristics

Transmitter/receiver	Remarks
Aperture diameter	Physical size of the instrument's aperture that limits transmitted and received beams.
Laser beam diameter and truncation factor	For a Gaussian beam, the laser beam diameter is defined as the diameter measured at $1/e^2$ in power at the lidar aperture. The laser beam diameter defines the illuminance level and so the eye safety. The truncation factor is the ratio between the diameter measured at $1/e^2$ and the physical size of the instrument's aperture.
Focus point	Usually pulsed lidars use collimated beams. For some applications, the beam can be partially focused at a given point to maximize the intensity on the beam laser within the measurement range. The intensity of the signal, and thus the velocity accuracy will be optimized at this specific point.

In principle pulsed systems are monostatic systems. For continuous wave systems also bistatic setups are available.

4.1.3 Signal sampling parameters

The sampling of the pulsed lidar signal in range is determined by the parameters given in Table 2.

Table 2 — Signal sampling parameters

Signal sampling parameters	Remarks
Range gating	The range gate positions can be defined along the line of sight.
Range gate width	Given by the sampling points or the sampling frequency of the digitizer. Must be chosen close to the pulse length.
Number of range gates	For real time processing, spectral estimation of all range gates must be computed in a time less than the integration time.
Radial window velocity measurement range	Wind velocities as low as 0.1 m/s can be measured with the aid of Doppler wind lidar systems. The measurement range is restricted towards the upper limit only by the technical design, mainly by the detection bandwidth. A radial wind velocity range of more than 70 m/s can be measured.
Resolution of the radial velocity	The wind velocity resolution is the minimum detectable difference of the wind velocity in a time and range interval. A resolution of 0.1 m/s or better can be achieved by averaging.

4.1.4 Pointing system characteristics

The pointing system characteristics are given in Table 3.

Table 3 — Pointing system characteristics

Pointing system characteristics	Remarks
Azimuth range	When using a pointing device, a lidar has the capability to point its laser beam at various azimuth angles with a maximum angular capability of 2π. For endless steering equipment, a permanent steering along the vertical axis is allowed. Other scanning scenarios should be followed for non-endless rotation gear.
Elevation range	The pointing device can be equipped with a rotation capability around the horizontal axis. Potential 360° rotation can be addressed. Typical elevation angles are set from 0° to 180° in order to observe the semi-hemispherical part of the atmosphere above the lidar. Anyhow, a nadir pointing can be used for resting position of the equipment.
Angular velocity	The angular velocity is the speed at which a pointing device is rotating. A measurement can be performed during this rotation. In this case, the wind velocity information will be a mean of the various lines of sights in the probed area, between a starting angle and a stopping angle. Other scenarios of measurement can use a so called step and stare strategy, with a fixed position during the measurement.
Angular acceleration	Defines how fast the angular velocity can change. To be defined for complex trajectories with fast changes in direction. Angle overshoots can be observed at high angular acceleration.
Pointing accuracy	The relative pointing accuracy is the standard deviation of the angular difference between the actual line of sight position (azimuth and elevation) and the position of the target (system of reference of the instrument). The absolute pointing accuracy needs prior calibration by angular sensors (pitch, roll, heading) (system of geographical reference).
Angular resolution	Minimum angle step that the line of sight can move. It can be limited by a motor reduction factor, position, encoder or mechanical friction.

4.2 Relationship between system characteristics and performance

4.2.1 Figure of merit

A figure of merit (FOM) helps to compare range performance of different lidars with different parameters. The example below allows the classification of pulsed lidar sensitivities, independently of atmospheric parameters. FOM is derived from the lidar equation (Formula (4)) and is proportional to velocity spectrum *CNR*, which is defined on the averaged spectral density as the Doppler peak intensity divided by the spectral noise standard deviation, assumed to be constant (white noise). *N* is the number of averaged pulses.

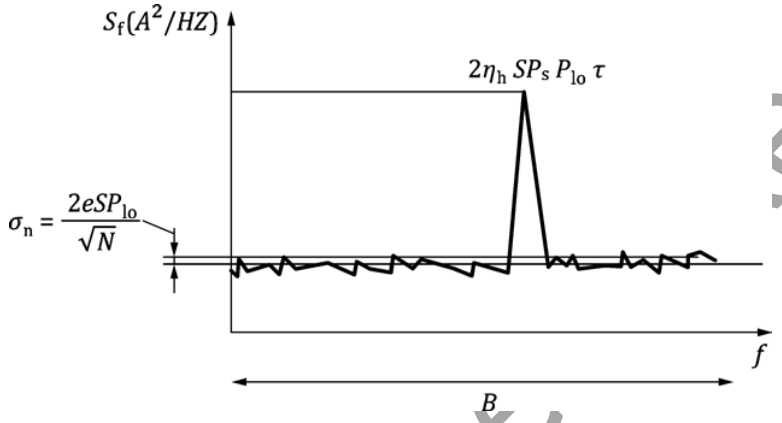

Figure 4 — Example of FOM

FOM is defined for a set of lidar parameters as:

$$FOM = \eta_{all} \cdot \mathrm{E} \cdot T_p \cdot D^2 \cdot \sqrt{t_i \cdot f_{PRF}} \quad (17)$$

Where

η_{all} is the overall efficiency, taking into account beam and image quality, overall transmission, truncation factor;

E is the laser energy at the laser output (received energy is proportional to peak power and laser footprint);

T_p is the pulse duration (this term comes from narrow bandwidth, inversely proportional to T_p);

D is the collecting telescope diameter (for typical long range applications the optimum is 100 mm to 150 mm in size for NIR wavelengths);

t_i is the integration time for one line of sight;

f_{PRF} is the pulse repetition frequency.

The FOM is proportional to the square root of number N of accumulated spectra: $N = t_i \cdot f_{PRF}$.

When comparing two lidars at two different wavelengths, spectral dependence of atmospheric parameters must be considered. The FOM must be calculated with an integration time less or equal to 1 second to avoid that wind or turbulence may fluctuate more than the Doppler spectral width.

A lidar may increase its FOM with a longer accumulation time within this 1s time limit.

Considering state-of-the-art low aberration optical components, η_{all} can be estimated by the product of the emitting path transmission by the receiving path transmission.

It has to be noted that the FOM for a pulsed Doppler lidar may not be increased indefinitely by increasing the collecting area D^2, since phase distortion across the beam due to refractive index turbulence degrades the heterodyne efficiency [3]. A practical limit is in the vicinity of D=125 mm useable diameter for long range lidars.

Since the velocity spectrum CNR, is inversely proportional to the squared range, the maximum operational range is approximately proportional to the square root of FOM, when atmospheric absorption can be neglected. When FOM is expressed in mJ ns m², the maximum operational range, expressed in km, is almost the square root of FOM.

Table 4 computes the FOM for typical lidar figures and their corresponding typical measurement range.

Table 4 — Figure of merit for typical lidar figures and their corresponding typical measurement range

η	E (mJ)	T_p (ns)	D(m)	f_{PRF} (Hz)	t_i (s)	FOM (mJ ns m²)	Typical measurement range (km)
0.5	0.2	800	0.12	10000	1	115	10
0.5	0.1	400	0.06	20000	1	10	3
0.5	2	300	0.12	750	1	118	10

4.2.2 Time-bandwidth trade-offs

A good practice is to match the pulse duration with the desired range gate (see Clause 3.6), so that the spatial resolution depends equally on these two parameters. With this assumption, spatial resolution is proportional to pulse duration. The shorter the pulse, the better the resolution. Velocity resolution is proportional to spectrum width and is larger when the spectrum is narrow. Because the spectrum width is inversely proportional to the pulse duration, range resolution and velocity resolution are also inversely proportional.

4.3 Precision and availability of measurements

4.3.1 Radial velocity measurement accuracy

Radial velocity measurement accuracy is defined (according to ISO 5725-1) in terms of

— trueness (or bias) as the statistical mean difference between a large number of measurements and the true value;

— precision (or uncertainty) as the statistical standard deviation of a series of independent measurements. It does not relate to the true value.

Lidar data of good quality are obtained when the precision of the radial velocity measurements is higher than a target value (e.g. 1 m/s) with a predefined probability of occurrence (e.g. 95 %).

An error value (1σ) of 0.5 m/s can be regarded as adequate for typical meteorological applications and for wind measurements to determine the statistics of dispersion categories for air pollution modelling [13]. For wind energy applications the requirements may be higher (0.2 m/s).

4.3.2 Data availability

Data availability is defined as the ratio of data with precision *P* to the total number of data during a measurement period.

NOTE The availability of measurement data, i.e. the determinability of the wind profile is a function mainly of the aerosol concentration and the clouds. Other filtering criteria may be applied, depending on the required data accuracy; for example, data that exhibits significantly non-uniform flow around the scan disk should be rejected.

4.3.3 Maximum operational range

Assuming the lidar line of sight remains within the planetary boundary layer (i.e. no significant change of signal along the line of sight), Figure 5 shows a typical pulsed lidar data availability versus range plot.

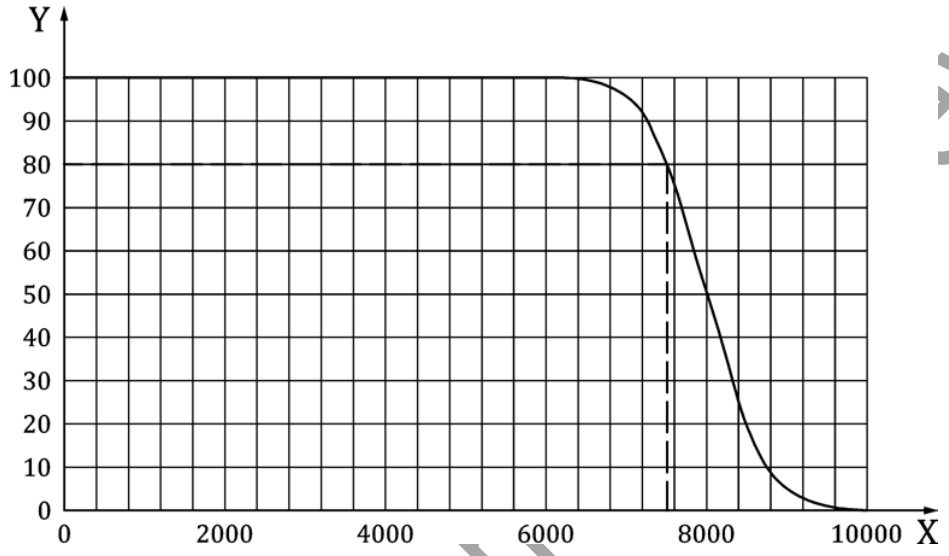

Figure 5—Example for maximum operational range (X: Range in meters, Y: Availability in %). In this case the range for 80 % data availability (P_{80}) is 7500 m

The performance shown in this diagram is based on a standard atmosphere:

— No clouds along the line of sight

— No precipitation

— Visibility over 10 km (clear air)

This performance will vary significantly with relevant local climatic and operational conditions. Data from greater ranges should be treated with caution, depending on the application.

Measurement range shall be defined with a given availability criteria. Recent study about this link is described in [14].

For example, R_{50} corresponds to the maximum range with availability over 50 %.

If the availability is not mentioned the Maximum Operational Range is supposed to be R_{80}, i.e. the maximum distance where the availability is over 80 %.

For a given availability a change in velocity precision leads to a change in maximum operational range.

4.4 Testing procedures

In order to accurately assess for the accuracy of the target variables, the manufacturer must perform a set of validation tests for the range and velocity. Some can be performed under laboratory conditions. Certain other validation tests can only be performed by a comparison with other reference instruments such as cup or sonic anemometers.

4.4.1 Radial velocity measurement validation

This section describes how the quality of radial velocity measurements can be checked and assessed.

4.4.1.1 Hard target return

This test consists in acquiring wind measurements with the beam directed to a stationary (unmoving) hard target (any building within lidar range) and checking the radial velocity measurement returned by the lidar is 0 m/s.

This test checks the frequency difference f_t - f_{lo} between emitted laser pulses and the local oscillator is known or determined with a sufficient accuracy (see Clause 3.5.3).

The range gate length must be close to the length of the laser pulse, and the distances of the range gates must be set so that the hard target is exactly at the center of one range gate, otherwise a velocity bias can occur in case of frequency drift within the pulse.

Hard target velocity measurements must be acquired during at least 10 min. The test is successful if the time sequence of hard target radial velocities is centred at about 0 m/s.

4.4.1.2 Self-assessment of radial velocity precision

In this test, the pulsed lidar beam is vertical and radial velocity measurements are acquired during at least 20 min at the rate of at least one profile of radial velocities every second. Let us denote by $v_r(x,k), k = 1, \dots, K$ the time sequence of radial velocities measured at distance x. The test consists in forming the power spectrum of the time sequence:

$$V(x,f) = \frac{1}{K}|\sum_{k=1}^{K} v_r(x,k) exp(-2j\pi f k \delta t)|^2 \quad (18)$$

Where

δt is the constant time lag between successive v_r

On average, the power spectrum $V(x,f)$ should look like Figure 6. At low frequencies, the power spectrum is dominated by natural wind fluctuations and shall follow a $f^{-\frac{5}{3}}$ law. At high frequencies, the power spectrum is dominated by the flat level of measurement errors (white noise). The level of this flat part directly gives the variance of these measurements $\sigma_e^2(x)$.

NOTE The test shall be carried out at night when the natural variability of the wind is weak, i.e. when the wind is considered to be calm. It may then happen that measurement errors are much larger than natural wind fluctuations so the $f^{-\frac{5}{3}}$ part of the power spectrum is hidden.

Fully described in [15] this technique allows for the estimation of the measurement precision of the lidar without any ancillary data.

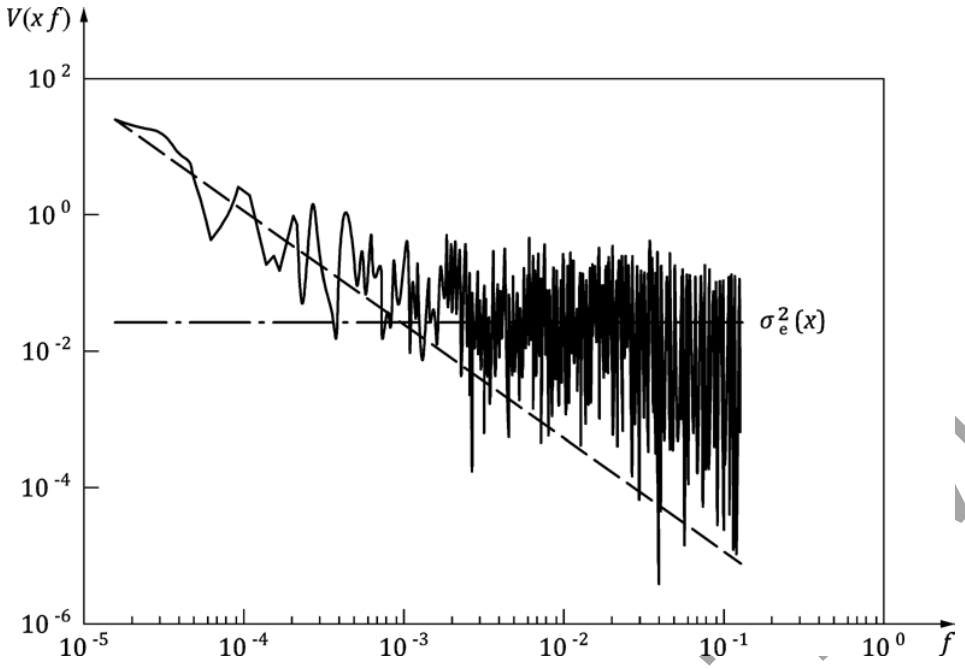

Key

f frequency

$V(x,f)$ power spectrum

Figure 6—Power spectrum of radial velocity measurements. The blue line is *V*(*f*). At low frequencies, *V*(*f*) should be proportional to $f^{-5/3}$ (spectral behaviour of natural wind variability – see green dashes). At high frequencies, the spectrum becomes flat (red dash-dot line) at a level directly equal to the variance of measurement errors $\sigma_e^2(x)$

4.4.2 Assessment of accuracy by intercomparison with other instrumentation

4.4.2.1 Sonic anemometer

The last test consists of directing the lidar beam very close to a sonic anemometer on a mast or platform without vibration and comparing lidar radial velocities with the projection of the three-dimensional wind vectors acquired by the sonic anemometer on the beam direction.

Lidar and sonic anemometer data shall be averaged over a minute.

The direction of the lidar beam shall be determined with a good accuracy (of the order 1° or better) and as close as possible to the horizontal plane. The lidar beam shall be at the height of the sonic anemometer (height difference of the order of 1 m or less).

The root mean square of the differences between lidar and sonic anemometer data shall be less than 0.1 m/s.

The mast will most likely cause wind flow perturbations downstream. Winds coming from directions such that the sonic anemometer is in the perturbed zone shall be removed from the statistics.

4.4.2.2 Performance test against masts

The mast shall be equipped with at least three cup anemometers mounted horizontally.

4.4.2.3 Comparison with Doppler weather radars

The possibility for intercomparison between Doppler lidars and Doppler weather radars can be an option where the two systems are collocated. The details about this class of intercomparison are just becoming known as the deployment of systems integrating both sensors for all-weather remote sensing of the wind field at airports, especially for wind shear detection, is just getting under way. Studies have recently been conducted [16;17;18]. Both sensors must be collocated and must probe the same atmospheric volume in order to be certain of representative intercomparisons.

In addition to the siting requirement, it is very important that weather situations be selected in which the tracer targets of both sensors actually represent the flow of air. In conditions of dry weather, the Doppler lidar works best, while under such conditions of clear air the radar measures only the returns due to scattering by insects. These scattered signals from insects provide no accurate indication of the actual air movement. Comparison with data from Doppler lidars typically show differences of up to several meters per second. Therefore, echo classification in terms of radar targets has to be enabled in order to be able to reject insect returns. This means that the radar has to be capable of measuring at two orthogonal linear polarizations. During precipitation events, however, conditions are optimal for the radar, whereas the lidar may have significantly reduced range coverage. In weather situations with light rain or drizzle from stratiform cloud, both radar and lidar sensors are expected to obtain high quality data; such situations are thus best suited for this validation procedure. Appropriate filtering of radar data on the basis of target classification using dual polarization moments needs to be conducted in order to get rid of any non-meteorological returns.

If these requirements are fulfilled, cross comparison of Doppler weather radar and Doppler lidar can be performed on the basis of profiles of horizontal wind as obtained e.g. with velocity volume processing (VVP) or velocity azimuth display (VAD) methods; In this case the scan geometry has to be considered. Ideally, the scan geometry for the radar and lidar should be the same with respect to elevation angles. Another option yet to be evaluated could be to compare the actual radial wind velocities on a range gate by range gate basis between the radar and lidar systems.

4.4.2.4 Comparison with radar wind profilers

Comparison with radar wind profilers may be performed if the two systems are collocated. The weather conditions under which both sensors work optimally are not exclusive of each other (sufficient aerosol tracers for lidar and sufficient turbulent eddies as targets for Bragg scattering for the wind profiler). Care must be taken that both sensors face optimal atmospheric conditions. Additionally, attention has to be paid to the scan mode used to derive the vertical wind profile so that the volume probed by the lidar matches the volume probed by the wind profiler.

4.4.3 Maximum operational range validation

In clear sky conditions the atmosphere can be described by the visibility V, the aerosol concentration and the aerosol type, where the last two can be properly described by the two optical lidar parameters extinction and backscatter coefficients. The visibility (see e.g. ISO 28902-1: Ground-based remote sensing of visual range by lidar) and humidity are measured by standard ground based meteorological local sensors whereas the aerosol type and its size distribution are not. To simplify, atmosphere types can be sorted in a few categories associated with their lidar ratio. Lidar Ratio values in the NIR typically are limited in the range of 30 to 50 steradians. R_{MaxO} will not be too dependent on the aerosol variability on site except for conditions with local pollution sources.

Visibility is an important parameter for lidar range. Lidar equation indicates that the received power is proportional to the backscatter coefficient and decreases exponentially with extinction, thus increases with visibility. Since $\alpha(x)$ and $\beta(x)$ are proportional, there is a maximum to the function $P_r(t)$ (see lidar equation (Formula (4)and Figure 7), and so for $R_{MaxO.}$

To discard unfavourable visibility conditions for coherent Doppler wind lidars (fog and very clear), only haze and clear visibility conditions are selected for range measurements. Current lidars can work in precipitating conditions, but are subject to error in their determination of the vertical wind component; the horizontal component has been shown to be very accurate (see [18]).

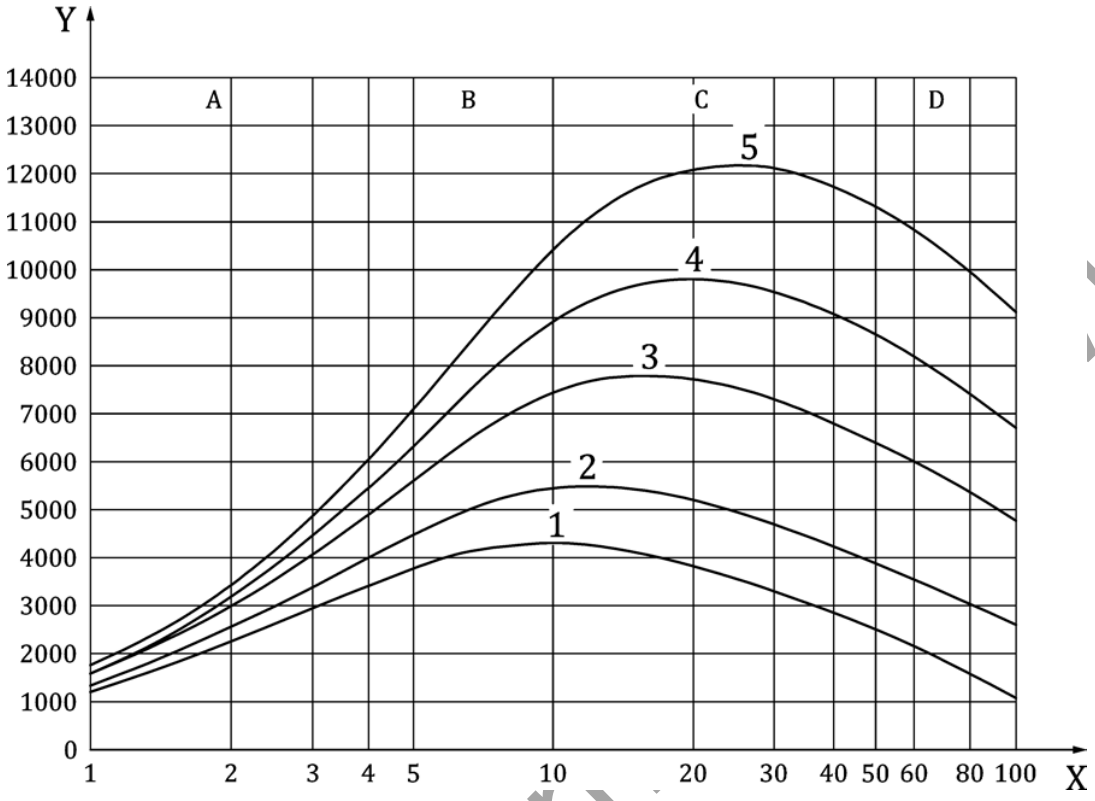

Figure 7—Dependency of the maximum operational range of the heterodyne Doppler signal to the visibility conditions (X: Visibility in km, Y: maximum range in metres, 1 to 5: different FOM values (see Table 5)). A: Fog; B: Haze; C: Clear; D: Very clear

Table 5 — Plot numbers

Plot number	1	2	3	4	5
Typical FOM for 1s integration time (mJ ns m²)	20	30	60	100	150

Because backscatter changes rapidly for high RH values, data corresponding to RH > 70 % must be filtered out the measurement data set. So, precipitation conditions (rain, snow) are not considered.

Moreover, index turbulence Cn^2 (depends on temperature and altitude) can modify R_{MaxO} by altering the beam wave front. Strong turbulent conditions must be removed from data sets (sunny days around noon), and experimental protocol must be followed up.

So the validation shall be conducted under the following conditions:

— The lidar is operated in operational conditions (vertical for profilers, low elevation for scanning lidars.
— The full measurement range remains in the boundary layer.
— 10 km < visibility < 50 km (at visible wavelength, dependency with wavelength is given in ISO 28902-1)
— No precipitation
— No cloud on the line of sight
— $Cn^2 < 10^{-14}$ $m^{-2/3}$ (1 m above ground level)

Data not corresponding to these conditions must be filtered out for assessing the maximum operational range.

— Context conditions are recorded simultaneously (temperature, Cn^2, visibility, RH)
— Data sets are created following the above mentioned atmospheric conditions. 100 h of filtered data are required as a minimum for a good statistical data set. It represents around four days of cumulated measurements with 1 s accumulation time. Depending on the atmospheric conditions the evaluation period can last from four days and up to one month.

5 Measurement planning and installation instructions

5.1 Site requirements

The selection of the measurement site is essentially determined by the measurement task. Careful selection of the measurement site is necessary, in particular, for stationary systems or for the quasi-stationary use of mobile systems during long-term measurement campaigns. The following points shall be taken into account when selecting the measurement site:

— Unobstructed view: Unrestricted visibility can be limited by built up areas, trees, buildings near the installation site of the lidar. If the view is limited by buildings it is possible to avoid the limitation of the horizontal view by selecting a larger elevation angle. In the case of a VAD scan, the measurement signals originating not from the free atmosphere but from obstacles shall be excluded from the evaluation.

— Electromagnetic radiation: Doppler wind lidar systems should be shielded properly against interferences by electromagnetic radiation (e.g. by radar, mobile radio or cellular phone networks).

Early inspection of the envisaged measurement site with the participation of experts (e.g. meteorologists) is recommended.

For optimal operational range retrieval, the lidar should be installed on a short grass covered ground with no nearby structures, which would cause atmospheric turbulence affecting the lidar's operation and performance. The lidar should be installed at least at 3 m above the ground, especially when not located on a grass ground, like concrete, asphalt or a plain metallic platform, in order to avoid effects from turbulence nearby the optical output that will destroy the coherency of the atmosphere and thus diminish drastically the detection.

5.2 Limiting conditions for general operation

Interference factors regarding Doppler wind lidar measurements are:

— optically thick clouds;
— precipitation of any type (rain, hail, snow);
— blocking effects (e.g. buildings).

5.3 Maintenance and operational test

5.3.1 General

To ensure the system functions as specified and to rule out deviations and technical errors such as maladjustments [19], maintenance and operational tests shall be performed in regular intervals.

5.3.2 Maintenance

Maintenance such as regular cleaning of the optical components, calibration etc. shall be performed as a basic requirement of quality assurance. Maintenance procedures may be conducted by on site personnel, using an automatic software detection of the decrease of the signal due to, e.g. dust deposits, and making appropriate corrections to the data, or a combination of the two. Typical maintenance intervals are three months depending on the environmental conditions.

5.3.3 Operational test

Operational tests should be performed every 6 to 36 months. The tests depend on the individual system design. The manufacturer shall specify the testing procedures and provide the necessary testing tools.

a) Output power and frequency of the laser source should be measured at the periodicity indicated by the manufacturer.

b) Signal output of the data acquisition system reacting to a defined light pulse or defined target should be measured at the periodicity indicated by the manufacturer.

c) For scanning or steering systems, an alignment test using a calibrated instrument (e.g. compass, inclination meter) should be performed.

5.3.4 Uncertainty

Table 6 compiles uncertainty contributions to the measurement variables and the line-of-sight wind velocity. The uncertainty contributions of the measurement variables influence the quality of the data produced by the system. The dominant uncertainties result from:

— the initial calibration process of the system by the manufacturer, and

— the prevailing environmental conditions.

Table 6 — Effects leading to uncertainty

Measurement variables	**Effects leading to uncertainty**
SNR	— Noise including detector noise — Speckle effect (when only a few pulses are averaged during the measurement time) — Laser power or pulse width fluctuations — Refractive index (temperature) turbulence Lag angle at fast rotation speeds
Frequency shift Δf	— Bias and fluctuations of emitted pulse frequency compared to local oscillator frequency — Pulse length — *SNR* — Number of averaged pulses — Quality of estimator
Target variable	**Uncertainty contribution**
line-of-sight wind velocity (radial wind velocity)	— Wind turbulence — Wind gradient along the line of sight — Hard targets close to the range gate — Range ambiguities — Pointing accuracy

Attachment A

(informative)

Continuous-wave Doppler wind lidar

As stated in this annex there are several methods by which lidar can be used to measure atmospheric wind. The four most commonly used methods are pulsed and continuous-wave (CW) coherent Doppler wind lidar, direct-detection Doppler wind lidar and resonance Doppler wind lidar (most commonly used for mesospheric sodium layer measurements).

This annex describes the use of heterodyne (coherent) pulsed lidar systems. It should be noted that there is also a Part 3 of ISO 28902 currently in preparation, which describes the use of continuous-wave coherent Doppler wind lidar for the measurement of atmospheric wind. Part 3 of ISO 28902 will specify the requirements and performance test procedures for continuous-wave Doppler lidar techniques and presents its advantages and limitations. The term "continuous wave Doppler lidar" or "continuous wave Doppler wind lidar" is used in this annex to apply to continuous-wave lidar systems making measurements of wind characteristics from the scattering of laser light by aerosols in the atmosphere within the low-altitude boundary layer. A description is provided of typical measurement geometries, signal-processing options, performance requirements, and limits based on standard atmospheric conditions. The applications for continuous wave lidar are, among other: wind energy; wind resource assessment; power curve verification; loss factor in the wind farm operation; wind hazards monitoring for aviation weather applications; wind shear; requirements for the detection of wake vortices behind aircraft.

Part 3 of ISO 28902 will address manufacturers of continuous-wave Doppler wind lidars as well as those bodies concerned with the testing and certifying their conformity. It will also provide recommendations for users to make adequate appropriate use of these instruments. A comprehensive bibliography of independent publications will be provided.

Attachment B

(informative)

Retrieval of the wind vector

B.1 General

The wind is a three-dimensional vector quantity, with the wind field being generally a function of space and time. The measurement of the instantaneous wind at a particular position therefore always requires the determination of three vector components. A single Doppler lidar is only able to measure the component (or projection) of the wind vector along the line of sight of the laser beam. Three separated lidar systems would therefore be required to perform an exact local measurement at any fixed time. Under certain assumptions it is possible to estimate the full wind vector from a single "monostatic" Doppler lidar. This process is called wind retrieval, since the accuracy of the wind vector estimate depends on the validity of the assumptions regarding the wind field.

B.2 The coordinate system

Figure B.1 shows the wind vector $\vec{u}(\vec{r},t)$ in the Cartesian coordinate system with the unit vectors $\vec{\imath},\vec{\jmath},\vec{k}$.The components u_X, u_Y, u_Z are scalar functions of position and time, $\vec{r}=\vec{r}(x,y,z,,t)$ is the position or radius vector of an air parcel.

$$\vec{u}=\frac{d\vec{r}}{dt}=\begin{pmatrix}u_x\\u_y\\u_z\end{pmatrix} \tag{B.1}$$

Or

$$\vec{u}=\left[u_x\cdot\vec{\imath}+u_y\cdot\vec{\jmath}+u_z\cdot\vec{k}\right] \tag{B.2}$$

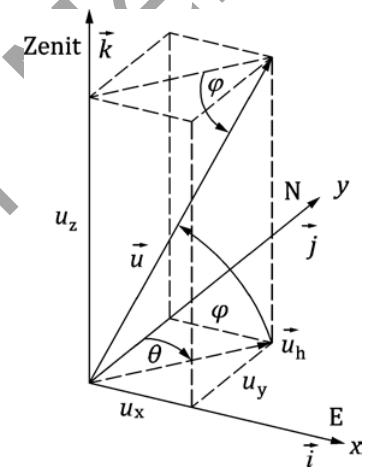

Figure B.1 — Coordinate system and wind vectors

The coordinate system in Figure B.1 points to the East (E) with the positive x-direction $(\vec{\imath})$, to the North (N) with the positive y-direction $(\vec{\jmath})$ and to the zenith with the positive z-direction $(\vec{k})$.

With $U=|\vec{u}|$, θ and ϕ, the components in Cartesian coordinates are:

$$\begin{aligned}u_x&=U\cdot\cos\phi\cdot\sin\theta\\u_y&=U\cdot\cos\phi\cdot\cos\theta\\u_z&=U\cdot\sin\phi\end{aligned} \tag{B.3}$$

and the three-dimensional wind vector becomes:

$$\vec{u} = \begin{pmatrix} U \cdot \cos\phi \cdot \sin\theta \\ U \cdot \cos\phi \cdot \cos\theta \\ U \cdot \sin\phi \end{pmatrix} \quad \text{(B.4)}$$

EXAMPLE Horizontal west wind: θ = 90°, φ= 0°

$\Rightarrow u_x = U,\ u_y = u_z = 0 \implies \vec{u} = (U, 0, 0)$

B.3 Horizontal wind vector

The horizontal wind vector $\vec{u}_h$, the horizontal projection of the three-dimensional wind vector $\vec{u}$ in Figure B.1 becomes:

$$\vec{u}_h = \begin{pmatrix} u_x \\ u_y \end{pmatrix} = \begin{pmatrix} u_h \cdot \sin\theta \\ u_h \cdot \cos\theta \end{pmatrix} \quad \text{(B.5)}$$

or, in component notation:

$$u_h = |\vec{u}_h| = U \cdot \cos\phi = \sqrt{u_x^2 + u_y^2} \quad \text{(B.6)}$$

The value u_h is denoted as horizontal wind velocity or colloquially as wind velocity. According to the meteorological convention, the wind direction is defined as the direction opposite to the wind vector $\vec{u}_h$. It is oriented clockwise from North via East, South and West (see Figure B.1).

For the case of a lidar scanning in a disk at fixed elevation angle in uniform wind flow, the individual line-of- sight velocity points follow a cosine form as a function of azimuth angle. The peaks of the function correspond to the azimuth angle aligned parallel or anti-parallel to the wind direction. The function passes through zero when the azimuth angle is perpendicular to wind bearing since there is no component of velocity along the line of sight. The data are also conveniently displayed on a polar plot, which provides information at a glance on the speed, direction and vertical wind component. A standard least-squares fitting routine provides the best estimates of the values of the three unknown parameters (either u, v and w, or alternatively horizontal speed, vertical speed and wind bearing).

B.4 Radial velocity

In lidar measurements, the component v_r of the local wind vector $\vec{u}(\vec{r}, t)$ in the beam direction of the laser, i.e. radial velocity at any arbitrary position $\vec{r}$ is the direct measurand determined from the Doppler frequency shift (see Figure 5). If the wind vector $\vec{u}(\vec{r})$ is written in a spherical coordinate system $(\vec{e}_r, \vec{e}_\theta, \vec{e}_\phi)$ instead of an Cartesian $(\vec{\imath}, \vec{\jmath}, \vec{k})$ coordinate system, the radial velocity v_r is easily defined (compare Formula (B.2)) [20]:

$$\vec{u}(\vec{r}) = \vec{u}(r, \theta, \phi) = \left[u_r \cdot \vec{e}_r + u_\theta \cdot \vec{e}_\theta + u_\phi \cdot \vec{e}_\phi\right] \quad \text{(B.7)}$$

Where

$\vec{e}_r$ is the unit vector in beam direction;

$\vec{e}_\theta$, $\vec{e}_\phi$ are the unit vectors in the azimuth and elevation direction;

u_r, u_θ, u_ϕ are the orthogonal wind vector components of the coordinate system carried along during the scanning operation.

The projection of the wind vector $\vec{u}(\vec{r})$ onto the beam direction i.e. the scalar product ($\circ$) can be

derived with Formula (B.7):

$$\vec{u}(\vec{r}) \circ \vec{e}_r = u_r \equiv v_r \equiv -v_{LOS} \quad \text{(B.8)}$$

v_{LOS} is equal by convention to the negative radial component v_r of the local wind vector at the position $\vec{r}$.The negative sign of v_{LOS} corresponds to the convention that in lidar systems the wind velocity is regarded as positive towards the laser.

With the known transformation relation between spherical and Cartesian coordinates [19], v_r can be expressed by the Cartesian wind components u_x, u_y, u_z the result being:

$$v_{LOS} = -v_r = -\left(u_x \cdot \cos\phi \cdot \sin\theta + u_y \cdot \cos\phi \cdot \cos\theta + u_z \cdot \sin\phi\right) \quad \text{(B.9)}$$

B.5 Retrieval of the wind vector

The atmosphere must be sensed at different angles in order to detect the (Cartesian) components u_x, u_y, u_z of the wind vector[3] with the Doppler wind lidar. However, all wind components are usually subject to spatial and temporal fluctuations since the wind field in general cannot be regarded as homogeneous and stationary due to a variety of small scale atmospheric processes like gravity waves, convection, turbulence or orographically induced flow effects. Homogeneity assumptions must therefore be made in order to retrieve an estimate of the wind vector from the radial components. The better this assumption holds, the more does the estimate represent the actual wind field. The problem has been extensively discussed in the literature and is explained in textbooks for both radar and lidar, see e.g. [21;22].

Therefore, assuring that the wind field can be regarded as stationary over the measurement period and horizontally homogeneous over the sampled volume, that is if the wind field is only a function of the vertical coordinate *z*, then the radial wind measurements for a fixed geometrical height are given by the simple matrix equation:

$$A \cdot u = v_r \quad \text{(B.10)}$$

The rows of this (*n* x 3) matrix *A* are comprised of the unit directional vectors describing the pointing of the n beams. The vector v_r is also of dimension *n* and contains the radial winds obtained in the *n* pointing directions. This is nothing more than a compact notation for the *n* scalar (inner) products as given in (B.8). For *n* = 3, the inverse A^{-1} exists if *A* has rank 3 (e.g. all row vectors are linearly independent) and the wind vector can be directly obtained through:

$$u = A^{-1} \cdot v_r \quad \text{(B.11)}$$

For *n* > 3 and rank(*A*) = 3, the linear system is overdetermined and has usually either one solution or no (exact solution) at all. However, an approximate solution can be found which minimizes $\|A \cdot u - v_r\|^2$. This least-square solution can be expressed by the Pseudoinverse $(A^T A)^{-1} \cdot A^T$ of matrix *A*:

$$u = (A^T A)^{-1} \cdot A^T \cdot v_r \quad \text{(B.12)}$$

A^T denotes the transpose of matrix *A*. The equation is sufficiently general and describes all possible scanning configurations with n discrete beam pointing directions. Care must be taken in the practical use of this equation to obtain numerically stable implementations.

The Doppler Beam Swinging (DBS) technique or the Velocity Azimuth Display (VAD) scanning methods are two frequently used scan schemes for Doppler lidars.

In the case of the DBS technique, measurements are performed in at least three linearly independent directions. This method allows for a very fast scanning, but it may yield biased

[3] The wind components u_x, u_y, u_z are frequently also called *u*, *v*, *w*.

measurements if the wind field is non-homogeneous. The validity of the retrieval assumptions (homogeneity, stationarity) can be tested to some extend if more than three directions are used. An explicit example of the DBS method with n = 3 and n = 4 can be found in [23].

In the case of the VAD scan, the beam direction azimuth is varied in a continuous scanning operation. The variation of the azimuth angle during the measurement series yields a set of different projections of the local wind vector onto these measurement directions. The elevation angle remains constant in the process. Originally, the VAD method was proposed for a horizontally homogeneous wind field [24], later discussions were extended to allow for an additional linear variation of the vector components [25]. In the case of a homogeneous wind field, the result is a sinusoidal profile of the measured velocity v_{LOS}.

If the lidar is powerful enough to provide several azimuth scans at different elevations in reasonable time, these can be combined in order to compile a full volume scan. This makes it feasible to use a more elaborate model of the wind field that can be fitted to the vector of observations of v_r. That is, analogous to Formula (B.10) one can further expand the Taylor series incorporating also shearing of the wind, i.e. the first spatial derivatives. For Doppler Radars, this procedure is standard and is commonly known as Volume Velocity Processing (VVP). It has been originally published in [26]. This analysis then leads to Formula (B.13) instead of (B.10):

$$
\begin{aligned}
v_r = {} & \sin\theta \cdot \cos\phi \cdot u_0 + \cos\theta \cdot \cos\phi \cdot v_0 + \sin\phi \cdot w_0 \\
& + r \cdot \sin^2\theta \cdot \cos^2\phi \cdot u'_x \\
& + r \cdot \cos^2\theta \cdot \cos^2\phi \cdot v'_y \\
& + r \cdot \cos\theta \cdot \sin\theta \cdot \cos^2\phi \cdot \left(u'_y + v'_x\right) \\
& + \sin\phi \cdot (r \cdot \sin\phi - z_0) \cdot w'_z \\
& + \sin\theta \cdot \cos\phi \cdot (r \cdot \sin\phi - z_0) \cdot (u'_z + w'_x) \\
& + \cos\theta \cdot \cos\phi \cdot (r \cdot \sin\phi - z_0) \cdot \left(v'_z + w'_y\right)
\end{aligned}
\qquad \text{(B.13)}
$$

It should be noted that this model does not allow to extract any information about horizontal vorticity since u'_y and v'_x only appear as a sum in Formula (B.13). This method has been applied to lidar data and compared with Doppler weather radar data in [16].

Attachment C

(informative)

Applications

C.1 Wind energy

One of the main challenges in the wind energy market today is the optimal estimation of the future electrical output of a wind farm. Today, the procedure to estimate this is to have the best evaluation possible of the wind potential at a given site, the best evaluation of what a wind turbine can produce with the free wind that it receives and to properly evaluate the total production loss that can occur during the wind farm operation. Some of these losses can be due to the wakes, to the power performance loss of a wind turbine, downtime due to operation and maintenance of the wind farm and other parameters that can affect the global wind farm operation. Today, the ground-based coherent Doppler lidar is a suitable tool to be used during all the phases of the operation of a wind farm, from the development phase, to the commissioning, operation and repowering of old wind farms.

C.1.1 Wind resource assessment

Today the ground-based vertical-profiler lidar (both pulsed and CW types) is widely used in the wind energy market by all major developers in order to provide highly accurate wind speed data and reduce the horizontal and vertical uncertainty during the wind resource assessment campaign. Today ground based coherent Doppler lidar can be used without any mast during the campaign and this data are considered as bankable. Considering the size of the wind turbine and the height that they can reach, the lidar allows a proper evaluation of the vertical wind profile that is critical for the design of a wind turbine. The vertical wind shear (change in wind speed along the vertical axis) and the vertical wind veer (change in wind direction along the vertical axis) are two key elements to be considered that can affect the annual energy production of a wind farm.

The wind farms are moving more and more offshore, and today the ground-based pulsed-scanning lidar can be used for wind resource assessment campaign scanning offshore from the shore. This allows to decrease the horizontal uncertainty in the wind resource assessment campaign at a much reduced cost than the standard offshore met mast. In addition to this, the correlation of the wind measured with the scanning lidar can be used to validate some wind models for the wind transition offshore to the shore.

C.1.2 Power curve verification

Today IEC 61400-12-1 [27] mentions that a met mast is to be used for the power curve verification of a wind turbine. Considering the maturity of the ground-based lidar for the wind resource assessment application, IEC 61400-12-1 is in the process of evolving and will be including the ground-based lidar vertical profiler for power curve verification.

The power curve verification standard is also including a new measurement method by applying the rotor equivalent power curve. In this case, the entire wind profile of the rotor diameter is considered and used, in order to estimate the total incoming wind along a plane rather than only the wind coming at hub height.

In addition to the vertical profiler, when a wind turbine cannot be reached within the 2.5D distance of the free wind of the wind turbine (where D is the rotor diameter), the scanning ground-based lidar can also be used to perform some power curve verification, by scanning from the ground to the front of the wind turbine.

C.1.2.1 Loss factor in the wind farm operation

When globally looking at a wind farm, there are some loss coefficients that wind farm developers apply to their Annual Electrical Production output calculation, and the most accurate this information, the better the project and ease of financing.

The ground-based lidar is being used in a variety of programs for the validation of the wake loss deficit coefficient. Major wind farm developers / owners have their own wind flow modelling tool to optimize the wind farm design and layout, and today the ground-based lidar is the appropriate tool used to validate their model thanks to data generated by the lidar. In terms of optimization of the wind farm operation, the nacelle-based lidar is also widely used, for turbine control, yaw misalignment or nacelle anemometer calibration.

C.2 Wind hazards monitoring for aviation weather applications

According to the state of the art and the growth of the worldwide air traffic, several projects are going on over the world in order to renew and optimize the regulations of the Air Traffic Management ATM, like the Single European Sky ATM Research (SESAR) project in Europe [28] and the NextGen project in USA. In the field of aviation weather, two major applications have been highlighted: the measurements of wind shears and wake vortices. For these two applications, coherent Doppler lidars are now considered as well adapted and powerful sensors to improve the wind observations in order to increase safety and optimize the air traffic.

C.2.1 Wind shear

Wind shears are defined as significant changes of head- or tail- winds along the take-off path and the approach that can affect aircrafts [29]. These rapid changes in air speed cannot be balanced by acceleration or deceleration due to inertial effects. Thus, lift and drag and therefore the resultant flight path changes which is particularly dangerous near the ground. The effects of wind shear as mentioned above are particularly dangerous if they happen near the ground, i.e. during take-off or landing, where they can lead to severe accidents. This is why since the conference of Chicago, the International Civil Aviation Organization (ICAO) standards have taken care of the wind shears threats to civil air traffic by mentioning wind shears in Annex 3 [29] and by providing the manual No. 9817 for low level wind shears [30]. The Annex 3 distinguishes two aspects of wind shears: the wind shear alerts and wind shear warnings.

— Wind shear alerts consist in providing automatic alerts of wind shear intensity observed by ground- based remote sensors. The alerts are created once wind shears are above 15 kn (7.5 m/s) in terms of headwind/tailwind changes. As detailed in [30], the danger of wind shears is mainly due to the strong horizontal winds that induce strong headwind and tailwind changes for the aircrafts.

— Wind shear warnings shall give concise information on the observed or expected existence of wind shears which could adversely affect aircraft. They are focusing below 500 m and along take-off path and approach. They are prepared by the meteorological office in charge of the met observations at a given airport. The wind shear warnings will be prepared "manually" thanks to all the observations (ground- based, aircrafts) and weather forecasts available.

According to the best practices, described in [30], Coherent Doppler lidars are a good candidate technology for providing wind shear alerts and/or warnings since:

— The areas of interest are the take-off path and the approach that can be probed by a scanning coherent Doppler lidar with Plan Position Indicator PPI (typically with a 3° of elevation) or glide path [31] scans or lines of sights along glide path.

— The probing area for alerting wind shears is 2 extensions of 3 nautical miles NM of the runways that is to say a measurement range of 7 km at least. Measurement range must be 7 km at least in appropriate atmospheric conditions (described in Clause 4).
— The wind shears alerts are provided on the three boxes (of 1 NM) that compose the extensions of each side of the runways, commonly called the Arena (Area noted for

Attention). To compute differences of headwind or tailwind, two points are needed at a minimum. This corresponds to a theoretical required resolution better than 1.852 km. But, in order to get accurate wind shear alerts and to be able to monitor all the types of windshears and especially the smallest ones which are the microbursts (size > 1.5 km), a range resolution of 200 m is commonly used with lidars and radars.

— ICAO documents mention the typical alert frequency suitable for the wind shears detection. In worldwide best practices, this frequency varies from 1min to 3min.

— Above all, it is important to notice that the configurations (accumulation time, scanning speed, alert frequency) of an equipment like a lidar dedicated to wind shears alerts or warnings must be adapted to the local requirements specified by the air traffic controllers and by the local wind shears phenomena occurred.

Moreover, Doppler lidar systems compliant with requirements underneath should be considered as a valuable supplement to Doppler weather radar observations, since they have complementary performance with respect to precipitation. Doppler lidars perform best in clear air conditions when Doppler radar receives only weak signals and vice versa, when precipitation limits Doppler lidar observations, Doppler radar performs optimally. An example describing the set up at Hong Kong International Airport including a Doppler lidar can be found in [31].

C.2.2 Requirements for wake vortices detection behind aircrafts

There is strong interest of the Air Traffic Control ATC stakeholders for studying wake vortices because their strength (commonly characterized by their circulation) determines the minimum separation distance between aircrafts in order to ensure safety. Wake vortices consist in two strong horizontal rotational flows that trail from each wingtip. There are generated by the lift of the aircraft which induces air flow from below the wings around the wingtips into the region above the wings. The wake vortices are very stable compared to turbulence and they can last up to 3 min with stable atmospheric conditions. Their circulation is determined by the aircraft weight and air speed and by the wingspan. Their size is about 20 m but they can be very dangerous especially in the take-off and landing phases of flight.

That is why, since the 60s, regulations have been created by the ICAO to fix the separation distances between three categories. With the increase of worldwide air traffic and the development of super heavy aircrafts, several projects aim at renewing the ATC regulations and especially the separation distances. Thus plenty of wake vortices studies have been launched since the 90s in using computational fluid dynamic models and coherent Doppler lidar technology in order to optimize the separation distances while ensuring safety [32;33]. Scanning coherent Doppler lidars are particularly adapted to measure wake vortices since they allow to measure at high resolution below 10 m and at high frequency up to 5 s wake vortices generated by the aircraft below 500 m, for monitoring out of ground effects and in ground effect wake vortex behaviour. Usually wake vortices measurements are performed close to the runways with Runway Height Indicator RHI scans with narrow angles typically 10° to 40° to map vertically the motion of the wake vortices.

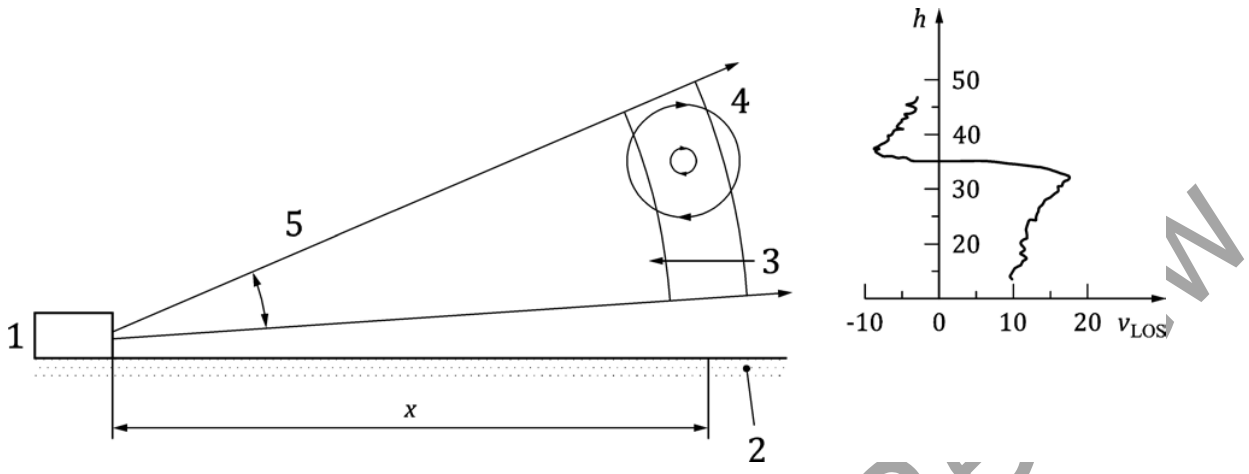

Key

1	Lidar
2	Runway
3	Cross wind
4	Vortex
5	Elevation scan

Figure C.1 — Measurement principle for determining aircraft wake vortices with Doppler wind lidar

Lidar measurements can besides be post-processed to calculate wake vortices characteristics like the probability of detection, the localization of their cores and their circulation (strength) [34;35].

C.2.3 Siting constraints

Since the Doppler lidar delivers only the radial wind speed, siting of the instrument is a crucial point, because runway oriented wind has to have a significant projection onto the line of sight of the lidar. In general, the magnitude, and therefore the quality, of the runway oriented wind component projected onto the line of sight deteriorates as $\cos^2\theta$, θ being the angle between the line of sight and the runway [6].

Another point is that ideally the 3° glide slope is to be scanned. This can be ideally done with one PPI scan, if the lidar is located at the runway threshold. If more than one runway threshold is to be monitored with one instrument, following exactly the 3° glide is not possible, and the above mentioned timing constraints usually do not allow scanning of more than one elevation. However, a 3° scan centred at the actual location of the lidar still outperforms an anemometer based Low-Level Wind Shear Alert System (LLWAS) in terms of glide slope wind shear detection.

Attachment D (informative)

Typical application ranges and corresponding requirements

Accordingly to the needs for the main applications (see Table D.1), three accuracy classes for the wind velocity are being defined. These classes are related to a defined spatial and temporal resolution. The wind velocity accuracy shall be ensured in all ranges of interest.

— Class A: $x \leq 0.1$ m/s (e.g. for wind energy purposes)

— Class B: $0.1 < x \leq 0.5$ m/s (e.g. for meteorological applications) [13]

— Class C: $0.5 < x \leq 1.0$ m/s (e.g. for nowcasting) [13]

Table D.1 — Typical application ranges and corresponding requirements

Application	Parameter to be provided	Reference	Typical probing range in m	Range resolution in m	Time resolution in min	Velocity measurement accuracy in m/s	Wind direction accuracy in °	Minimum data availability in %
Radial velocity mapping	Line of sight radial velocity	Formula (5)	200–10000	25–100	1–10	0.5	Not applicable	50–99[a]
Wind energy, e.g. — site assessment — power curve — wind profile	Profile of the horizontal wind vector along the vertical axis	e.g. [36]	40–200	25	10	0.5	2	85
High resolution NWP	Profile of the horizontal wind vector along the vertical axis	[13]	> 50	25	10	0.5	2	80
Air pollution, e.g. — dispersion modelling — risk management	Profile of the horizontal wind vector along the vertical axis	–	40–200	25	10	0.5	–	90
Aviation: wind shear	Radial wind along take off path, approach and runways	[29,36]	7000–8000 (5500 + half the runway)	200	1	0.5	5	80
Aviation: vortex monitoring (ground based systems)	Radial wind speed in perpendicular planes to the runway	–	Distance to runway + 300–500 on each side	25 (5 with overlap)	0.1	1	–	< 50
Met applications, e.g. — Nowcasting	Profile of the horizontal wind vector a vertical axis	[13]	0–4000	100	15	1	5	80

[a] depending on application

Bibliography

[1] Henderson, S. W., P. Gatt, D. Rees and R. M. N. Huffaker, 2005: Wind Lidar. In: Laser Remote Sensing, Editors T. Fujii and T. Fukuchi. 469-722, CRC Press, ISBN-10: 8247-4256-7.

[2] Measures, R. M., 1992: Laser Remote Sensing: Fundamentals and Applications. Krieger Publishing, 524. ISBN-10: 8946-4619-2.

[3] Frehlich, R., and M. Kavaya, 1991: Coherent laser radar performance for general atmospheric refractive turbulence. Appl. Opt., 30: 5325–5352.

[4] Belmonte, A., 2003: Analyzing the efficiency of a practical heterodyne lidar in the turbulent atmosphere: telescope parameters. Opt. Express., 11: 2041–2046.

[5] Frehlich, R., S. Hannon and S. Henderson, 1997: Coherent Doppler lidar measurements of winds in the weak signal regime. Appl. Opt. 36:3491–3499.

[6] Banakh, V. A. and I.N.Smalikho, 1997: Estimation of the turbulence eddy dissipation rate from the pulsed Doppler lidar data. Atmos. Oceanic Opt. 10 (12).

[7] Frehlich, R., 1996: Simulation of coherent Doppler lidar performance in the weak signal regime. J. Atmos. Ocean. Technol. 13:646–658.

[8] Dabas, A., P. Drobinski and P. Flamant, 2000: Velocity Biases of Adaptive Filters in Heterodyne Doppler Lidar Measurements. J. Atmos. Ocean. Technol. 17:1189–1202.

[9] Dabas, A., 1999: Semi empirical model for the reliability of a matched filter frequency estimator for Doppler lidar. J. Atmos. Ocean. Technol. 16:19–28.

[10] Goodman, J. W., 1975: Statistical Properties of Laser Speckle Patterns. In: Laser Speckle, (Dainty J.C., ed.). Springer.

[11] ANSI Z136.1-2014: American National Standard for Safe Use of Lasers. ISBN: 978-1-940168-00-5

[12] IEC 60825-1:2014: Safety of laser products – Part 1: Equipment classification and requirement.

[13] World Meteorological Organization: http://www.wmo-sat.info/oscar/requirements.

[14] Boquet, M., P. Royer, J.P. Cariou, M. Machta and M. Valla, 2016: Simulation of Doppler Lidar Measurement Range and Data Availability, Journal of Atmospheric and Oceanic Technology, paper accepted , DOI: 10.1175/JTECH-D-15-0057.1.

[15] Frehlich, R., 2001: Estimation of Velocity Error for Doppler Lidar Measurements. J. Atmos. Ocean. Technol. 18:1628–1639.

[16] Ernsdorf, T., B. Stiller, B.R. Beckmann, A. Weipert, S. Kauczok and R. Hannesen, 2014: Inter-comparison of X-band radar and lidar low-level wind measurement for air traffic control (ATC). 8th Europ. Conf. on Radar in Meteorol. And Hydrol., Garmisch-Partenkirchen, Germany.

[17] Hannesen, R., S. Kauczok and A. Weipert, 2014: Quality of clear-air radar radial velocity data: Do insects matter? 8th Europ. Conf. on Radar in Meteorol. and Hydrol., Garmisch-Partenkirchen, Germany.

[18] Weipert, A., S. Kauczok, R. Hannesen, T. Ernsdorf and B. Stiller, 2014: Wind shear detection using radar and lidar at Frankfurt and Munich airports. 8th Europ. Conf. on Radar in Meteorol. and Hydrol., Garmisch- Partenkirchen, Germany.

[19] Jörgensen, H., T. Mikkelsen, J. Streicher, H. Herrmann, C. Werner and E. Lyck, 1997: Lidar Calibration Experiment. Appl. Phys. B. 64:355–361.

[20] Bronstein, I.N., K.A. Semendjajew, G. Musiol and H. Mühlig, 1993: Taschenbuch der Mathematik. Harri Deutsch.

[21] Fukao, S. and K. Hamazu, 2013: Radar for Meteorological and Atmospheric Observations. Springer.

[22] Banakh, V.A. and I.N. Smalikho, 2013: Coherent Doppler Wind Lidars in a Turbulent Atmosphere. Artech House.

[23] Srinivaso, R.I., V.K. Anandan and R.R. Narasimha, 2008: Evaluation of DBS Wind Measurement Technique in Different Beam Configurations for a VHF Wind Profiler. J. Atmos. Ocean. Technol. 25 (12):2304-2312..

[24] Lhermite, R.M., 1962: Note on wind variability with Doppler radar. J. Atmos. Sci. 19(4):343-346.

[25] Browning, K.A. and R. Wexler, 1968: The determination of kinematic properties of a wind field using Doppler radar. J. Appl. Meteorol. 7(1):105-113.

[26] Waldteufel, P. and H. Corbin, 1979: On the analysis of single Doppler radar data, J. Appl. Meteor. 18:532– 542.

[27] IEC 61400-12-1:2005 Wind turbines – Part 12-1: Power performance measurements of electricity producing wind turbines.

[28] ATM MasterPlan, 2009: https://www.atmmasterplan.eu/.

[29] International Civil Aviation Organization, 2007. Annex 3 to the Convention on International Civil Aviation. Meteorological Service for International Air Navigation.

[30] International Civil Aviation Organization, 2005: Doc 9817 AN/449 Manual on Low-Level Wind Shear.

[31] Shun, C.M. and P.W. Chan, 2008: Applications of an Infrared Doppler Lidar in Detection of Wind Shear. J. Atmos. Ocean. Technol. 25(5):637-655.

[32] Wakenet-Eu. http://www.wakenet.eu/.

[33] Lang, S. and W. Bryant, 2006: Vortex Research in the USA (WakeNet-USA). ATO-Air Traffic Organization. FAA.

[34] Holzäpfel, F., T. Gerz , F. Köpp, E. Stumpf, M. Harris M., Young R.I. and A. Dolfi-Bouteyre, 2003: Strategies for Circulation Evaluation of Aircraft Wake Vortices Measured by Lidar. J. Atmos. Ocean. Technol. 20(8):1183-1195.

[35] Dolfi-Bouteyre, A., B. Augere, M. Valla, D. Goular, D. Fleury and G. Canat G 2009: 1,55 µm Pulsed Fiber lidar for wake vortex detection (axial or transverse). Wakenet-Eu Workshop.

[36] Hasager C.B., D. Stein, M. Courtney, A. Pena, T. Mikkelsen, M. Stickland and A. Oldroyd, 2013: Hub Height Ocean Winds over the North Sea Observed by the NORSEWInD Lidar Array: Measuring Techniques, Quality Control and Data Management. Remote Sens. 5: 4280–4303.